Supporting information

Hollow and Concave Nanoparticles *via* Preferential Oxidation of the Core in Colloidal Core/Shell Nanocrystals

Karol Miszta[1†], Rosaria Brescia[1†], Mirko Prato[1†], Giovanni Bertoni[1,2], Sergio Marras[1], Yi Xie[1], Sandeep Ghosh[1], Mee Rahn Kim[1] and Liberato Manna[1]*

[1] Department of Nanochemistry, Istituto Italiano di Tecnologia (IIT), via Morego, 30, 16163 Genova, Italy

[2] IMEM-CNR, Parco Area delle Scienze 37/A, IT 43124 Parma, Italy

[†] K. M., R. B. and M. P. contributed equally to this work

Contents

Optical characterization

The effect of the etching agents on the optical absorption of solutions of core-shell $Cu_{2-x}Se/Cu_{2-x}S$ NCs (of different shapes) is reported here. The emergence of surface plasmon absorption in the NIR region is a clear indication of an oxidative process due to extraction of Cu(I) ions and electrons from the NCs upon reaction with the tested etching agents.

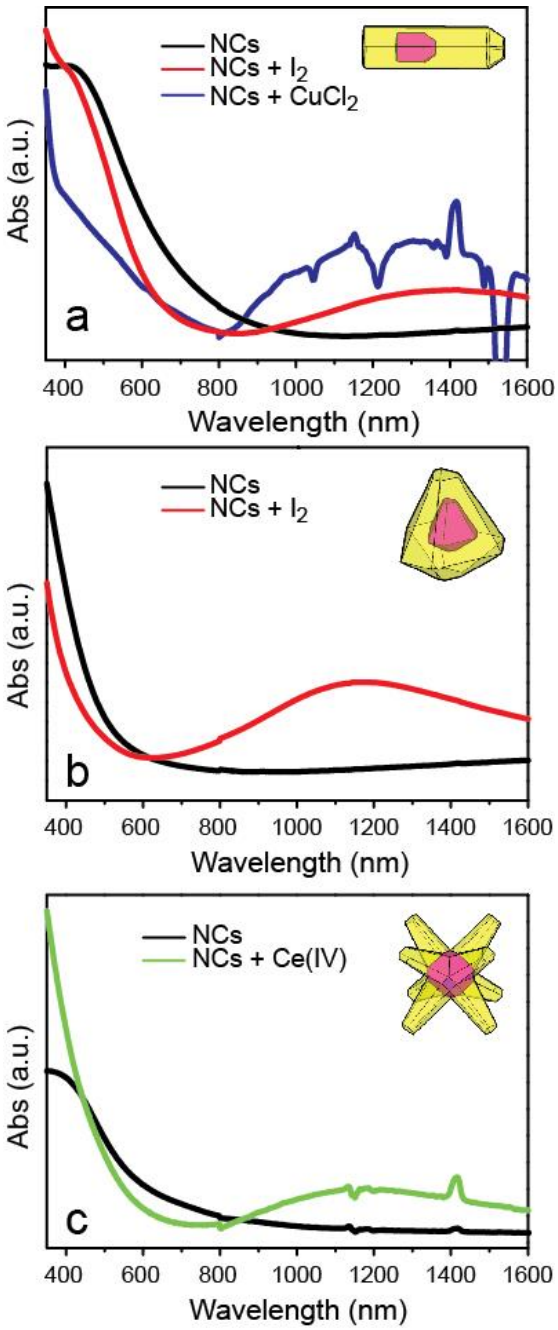

Figure S1: a) absorbance of a solution of bullet-in-rod $Cu_{2-x}Se/Cu_{2-x}S$ core/shell NCs before (black curve) and after addition of a few μL of solution of etchant: I_2 in toluene (red curve) or $CuCl_2$ in methanol (blue curve); b) absorbance of a solution of diamond-in-diamond $Cu_{2-x}Se/Cu_{2-x}S$ core/shell NCs before (black curve) and after addition of a few μL of I_2 solution in toluene (red curve); c) absorbance of a solution of octahedron-in-octapod $Cu_{2-x}Se/Cu_{2-x}S$ core/shell NCs before (black curve) and after addition of a few μL of solution of $(NH_4)_2Ce(NO_3)_6$ in methanol (green curve).

Effect of different etching agents: BF-TEM characterization

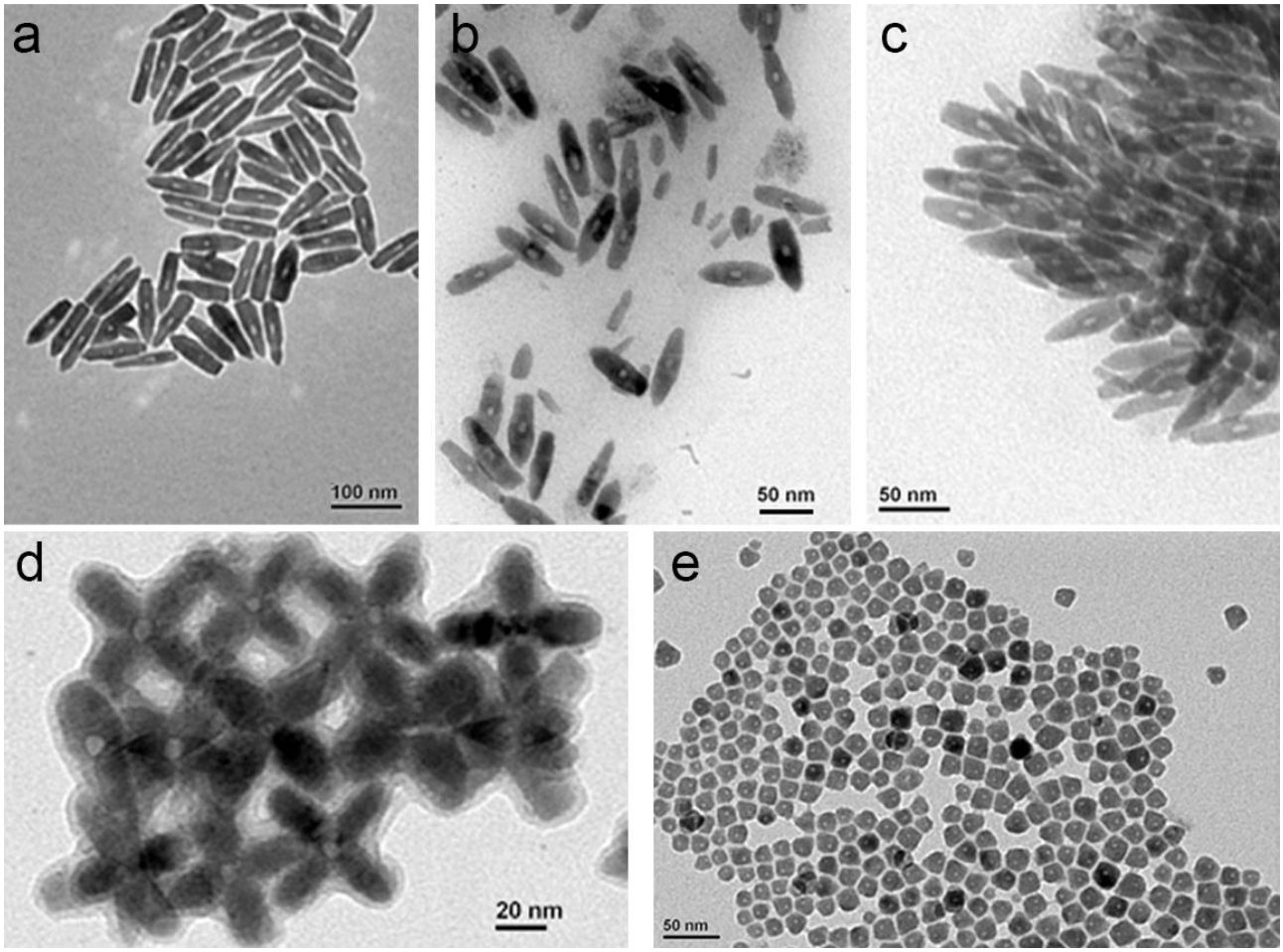

Figure S2: BF-TEM images of different shapes of nanocrystals upon exposure to various oxidative etching agents: a) bullet-in-rod $Cu_{2-x}Se/Cu_{2-x}S$ core/shell NCs after treatment with I_2 solution in toluene; b) bullet-in-rod $Cu_{2-x}Se/Cu_{2-x}S$ core/shell NCs after treatment with $FeCl_3$ solution in toluene; c) bullet-in-rod $Cu_{2-x}Se/Cu_{2-x}S$ core/shell NCs after treatment with HNO_3 solution (5%) in ethanol (experiment performed in air); d) octahedron-in-octapod $Cu_{2-x}Se/Cu_{2-x}S$ core/shell NCs after treatment with $(NH_4)_2Ce(NO_3)_6$ solution in methanol; e) diamond-in-diamond $Cu_{2-x}Se/Cu_{2-x}S$ core/shell after treatment with I_2 solution in toluene.

The etching experiments reported in Figure S2 were performed using freshly prepared stock solutions of cerium (IV) ammonium nitrate in methanol ($1.9x10^{-3}$ M), iron(III) chloride in methanol ($4.8x10^{-3}$ M), I_2 in toluene ($3.9x10^{-3}$ M), and HNO_3 (5%) in ethanol. The total concentration of Cu in the initial solutions of $Cu_{2-x}Se/Cu_{2-x}S$ NCs dispersed in toluene was determined by elemental analysis, *via* inductively coupled plasma optical emission spectroscopy (ICP-OES). Samples were prepared by adding etching solutions into the vials containing 100µL of NC solutions. The η values used to obtain the hollow crystals reported on Figure S2 were the following: 0.42 for Fig.S2a); 1.55 for Fig.S2b); 10 for Fig S2c); 3 for Fig. S2d); 1 for Fig. S2e). The prepared samples were precipitated, redispersed in toluene and deposited onto TEM grids under inert atmosphere (inside the glove box).

EDS line scan on diamond-in diamond NCs

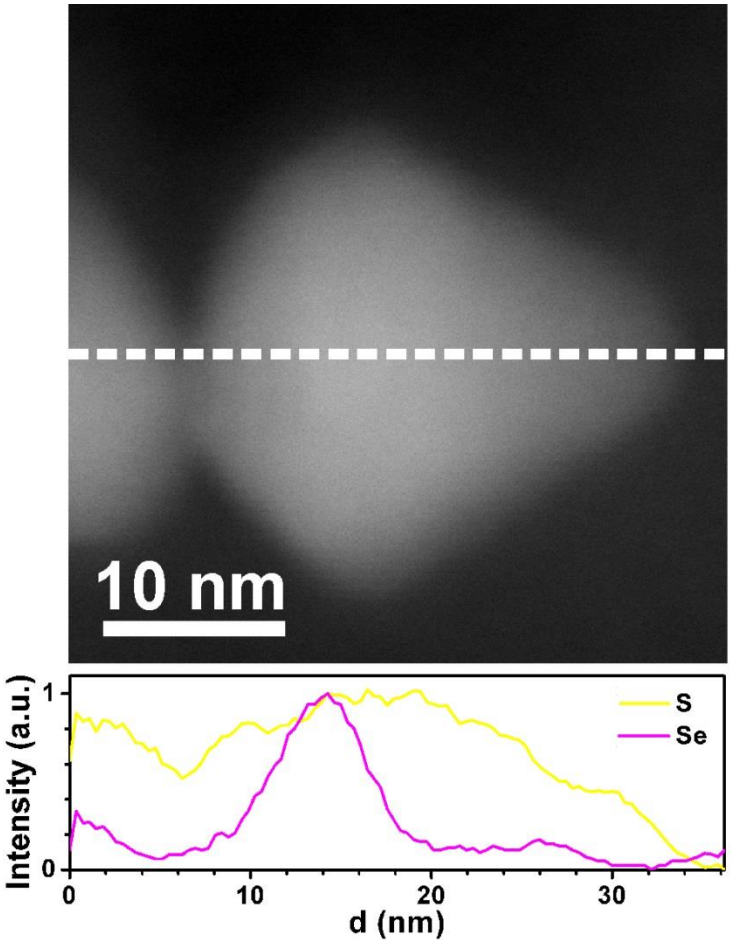

Figure S3: (top) HAADF-STEM image of a diamond-in-diamond $Cu_{2-x}Se/Cu_{2-x}S$ NC and (bottom) EDS line scan (S K and Se K integrated signals) along the dashed line, clearly showing the position of the $Cu_{2-x}Se$ core.

Etching evolution for octahedron-in-octapod NCs

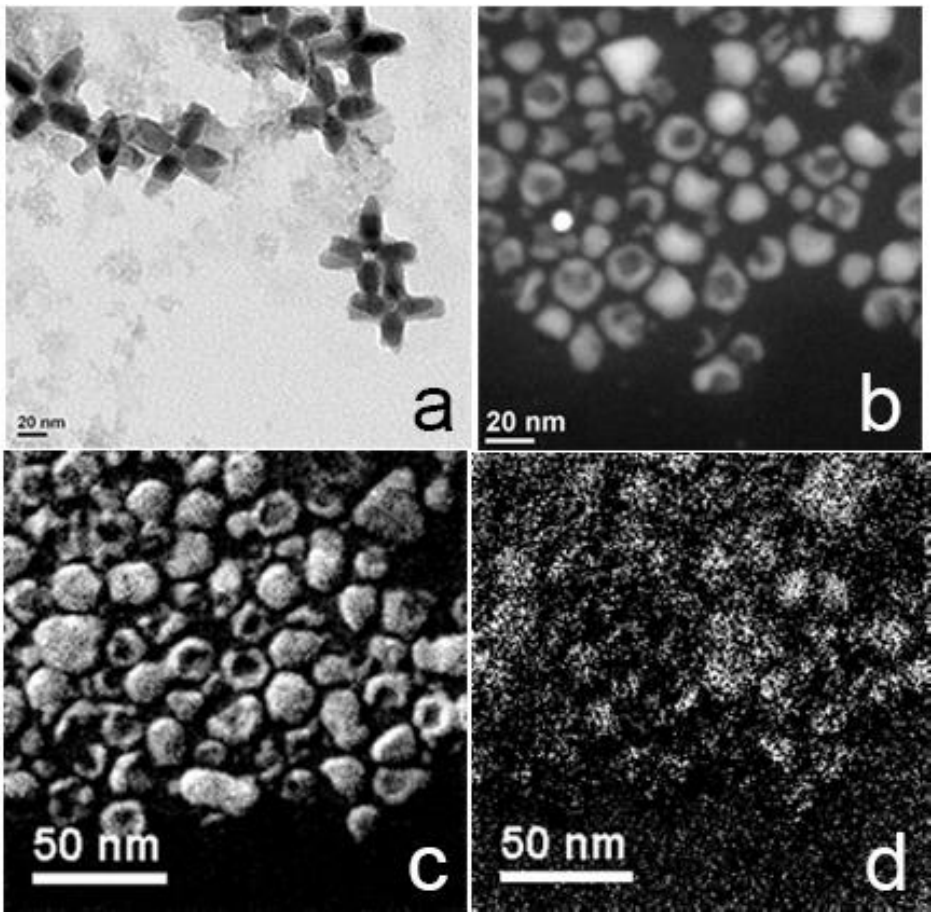

Figure S4: BF-TEM of a) octahedron-in-octapods NCs obtained after moderate etching (η between 2 and 4). The etching evolution of these NCs is similar to what shown for the bullet-in-rod ones: after the core region of the starting particles is consumed, the extremities of the NCs start being severely consumed and, eventually, only a porous $Cu_{2-x}S_ySe_{1-y}$ nanocage remains. HAADF-STEM analysis (panel b) shows that the inner part of the final nanocage resembles the shape of the original core. EFTEM images (panels c and d) shows that, also in the case of octahedron-in-octapods NCs, the final nanocage contains S (panel c, from S-$L_{2,3}$ edge at 165 eV) and Se (panel d, from Se-$L_{2,3}$ edge at 1436 eV). EDS analysis gave a S:Se average ratio on the particles close to 3:2.

Late stage of etching: nanocages of bullet-in-rod and octahedron-in-octapod NCs

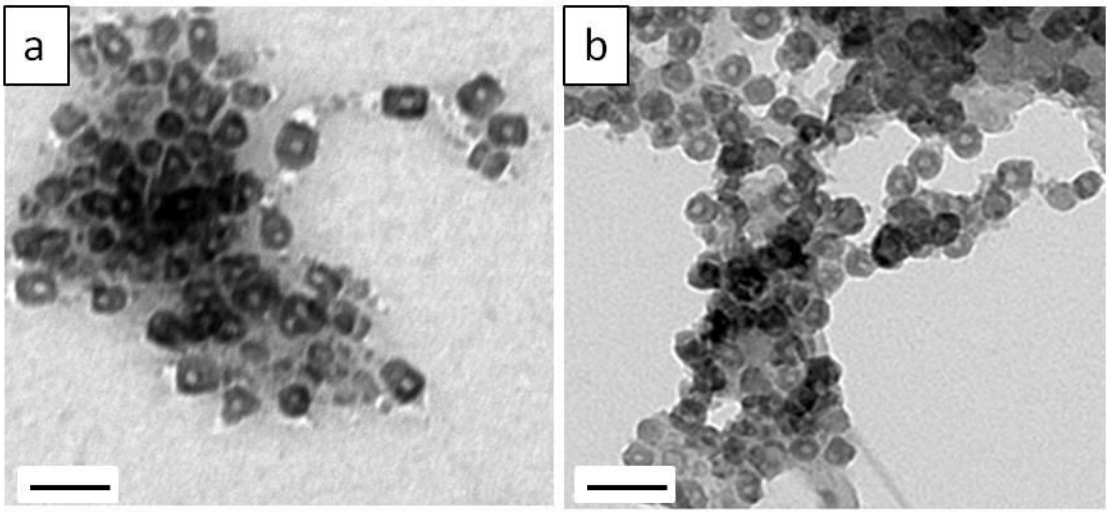

Figure S5: BF-TEM comparison of late stage of etching on a) bullet-in-rod NCs (η = 10) and b) octahedron-in-octapod NCs (η = 9).

XRD and SAED pattern on Cu-exchanged CdSe seeds for bullet-in-rod NCs

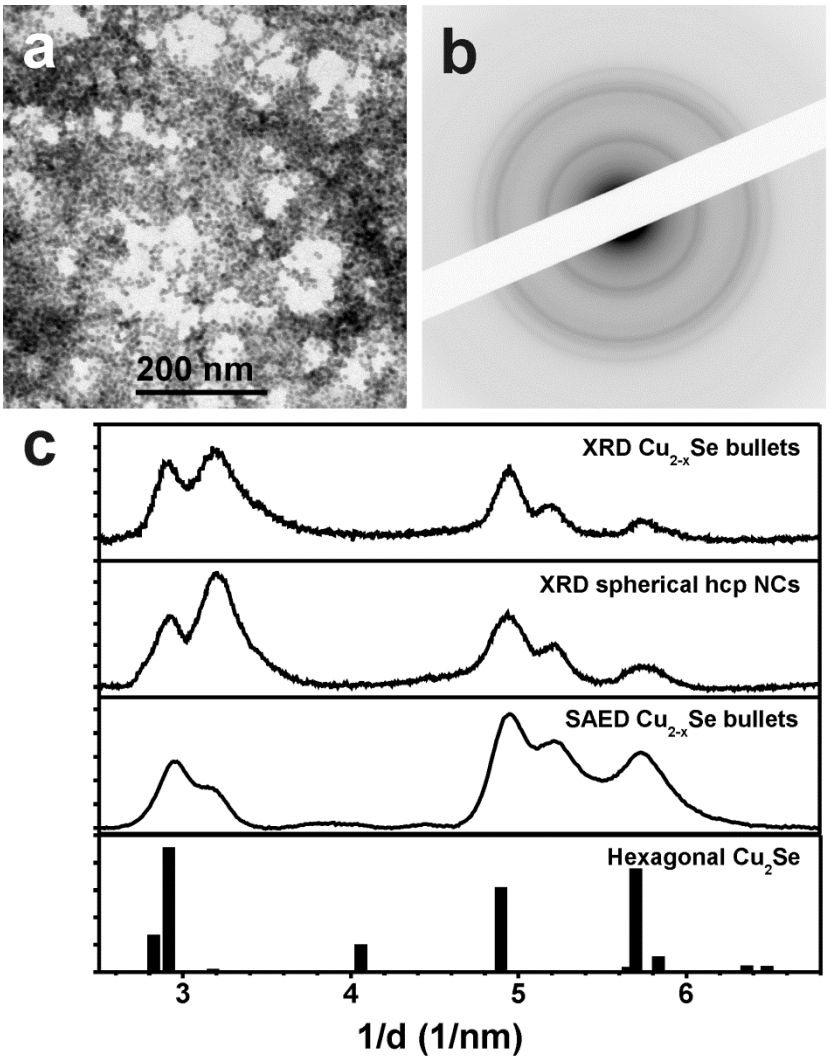

Figure S6: Diffraction analysis of $Cu_{2-x}Se$ bullet-like NCs obtained by cation exchange on CdSe NCs used for seeded growth of bullet-in-rod CdSe/CdS NCs. The details on synthesis and cation exchange are reported in the manuscript. (a) Overview BF-TEM image and (b) corresponding original (only inverted) SAED pattern. (c) XRD pattern, showing good agreement with the one reported for spherical hcp NCs in Fig. 5 of ref. 59 in the manuscript (H. Li et al., Nano Lett. 2011, 11, 4964), and azimuthally integrated SAED pattern (background-subtracted). As carefully verified in the mentioned reference, the XRD patterns are compatible with a hexagonal (β-chalcocite-like) Cu_2Se phase with expanded cell. The reference pattern at the bottom was calculated based on the ICSD database structure #20560 for β-chalcocite Cu_2S, using the cell parameters reported in the same reference (a = 4.09 Å, c = 6.86 Å) and replacing S atoms by Se atoms. Unlike what reported in the mentioned reference, the hexagonal Cu_2Se phase was stable under e-beam irradiation in the present experimental conditions (JEM1011 TEM, with thermionic W electron source operated at 100 keV acceleration voltage) due to milder irradiation conditions than those reported there (JEM 2200FS TEM, with Schottky FEG source operated at 200 keV acceleration voltage).

SAED pattern evolution with etching

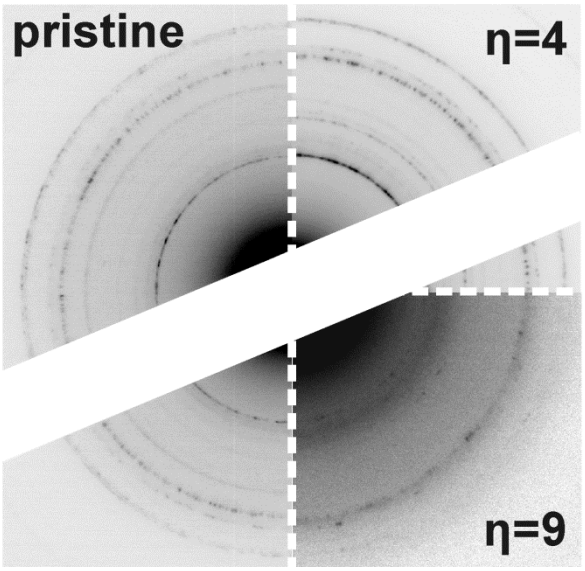

Figure S7: Original (only inverted) SAED patterns of groups of bullet-in-rod NCs from a pristine sample (left side), and of samples at moderate (η=4, top right panel) and late (η=9, bottom right panel) etching stages. The white bar in the center is the beam stopper used to protect the CCD camera from the high intensity of the undiffracted beam.

Large channels – concave NCs

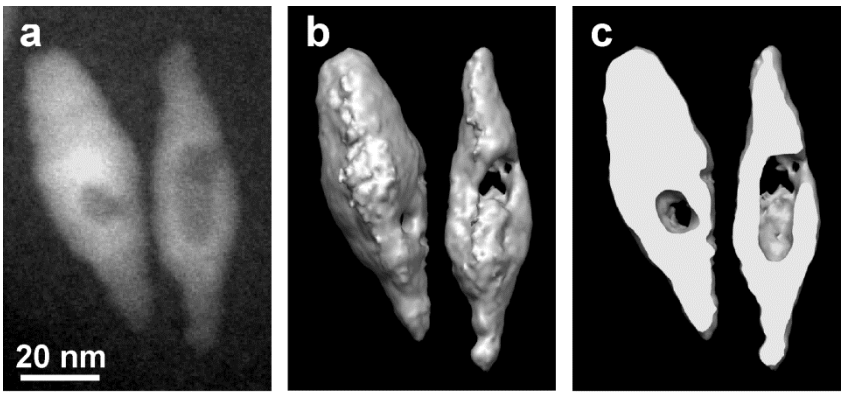

Figure S8: Electron tomography study of moderate etching stages of $Cu_{2-x}Se/Cu_{2-x}S$ bullet-in-rod NCs (η=4). (a) HAADF-STEM images of selected NCs and (b) isosurface rendering of the corresponding reconstructed volumes. The longitudinal cut-through in (c) evidences the presence of cavities of variable dimensions at this stage in different crystals.

XPS on bullet-in-rod NCs: early stage of etching

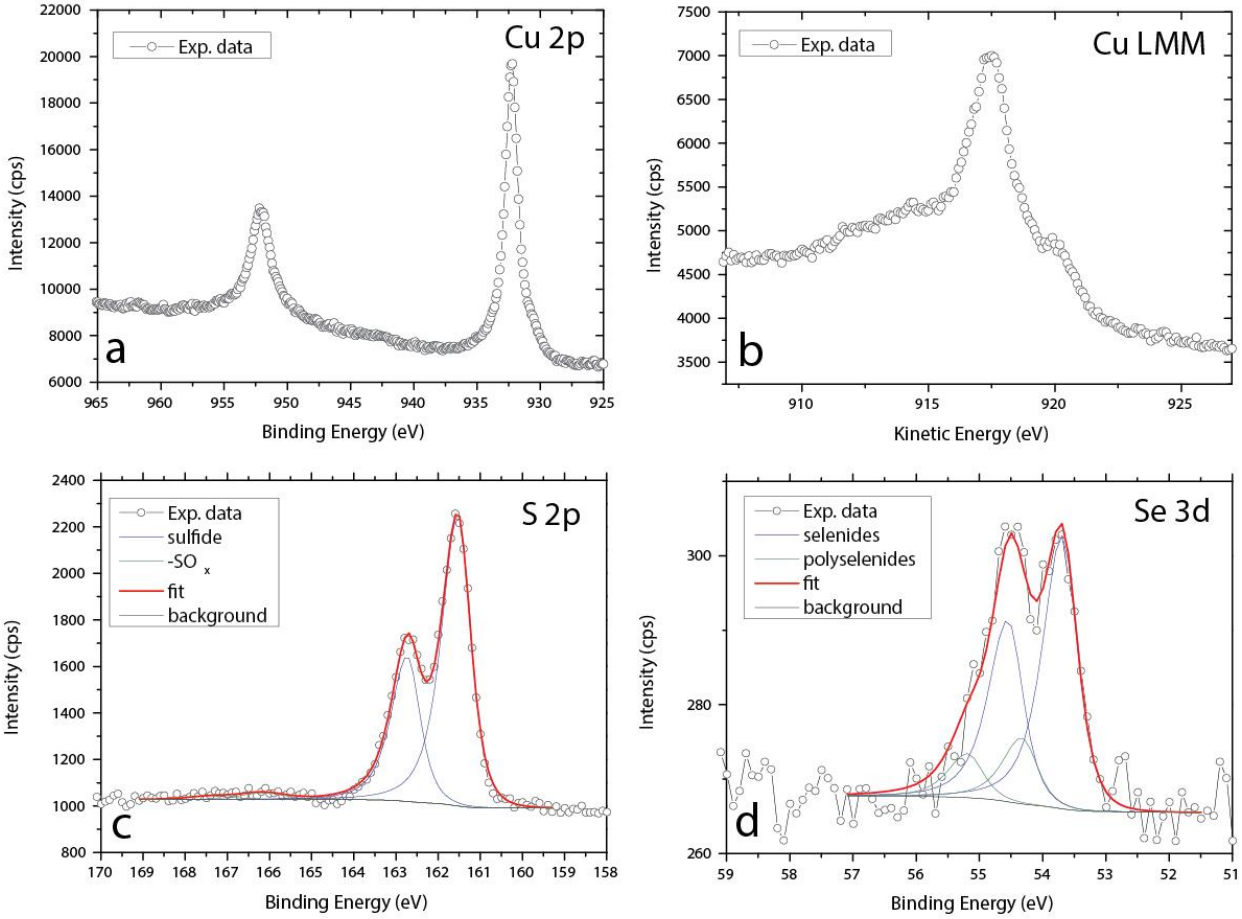

Figure S9: XPS characterization of bullet-in-rod NCs at early stage of etching (η = 1). The data are shown in the energy ranges typical for Cu (panel a and panel b), S (panel c) and Se (panel d) peaks. The position of the main Cu 2p peak at binding energy of 932.3 eV (panel a), together with that of the Cu LMM Auger peak (panel b) at a kinetic energy of 917.4 eV indicates the presence of Cu(I) species [J.F. Moulder, W.F. Stickle, P.E. Sobol, K.D. Bomben, Handbook of X-ray Photoelectron Spectroscopy, Perkin-Elmer Corp, Eden Prairie, MN, 1992].

S 2p data (panel c) were fitted with a single doublet (spin-orbit splitting = 1.2 eV; S $2p_{3/2}$/S $2p_{1/2}$ branching ratio of 2; S $2p_{3/2}$ peak centered at 161.5 eV), indicative of the presence of S^{2-} species [Y. Xie et al., J. Am. Chem. Soc., 2013, 135, 17630–17637].

On the other hand, the fitting of the Se 3d data required, in addition to the Se^{2-} doublet (spin-orbit splitting = 0.86 eV; Se $3d_{5/2}$/Se $3d_{3/2}$ branching ratio of 1.5; main peak at 53.7 eV) [S. Riha et al., J. Am. Chem. Soc. 2011, 133, 1383–1390], the presence of a second component (main peak at 54.3 eV), that could be correlated to oxidation state of Se higher than 2- (likely due to the presence of short polyselenides, as suggested by S. Riha et al.).

Reversed core/shell heterostructures

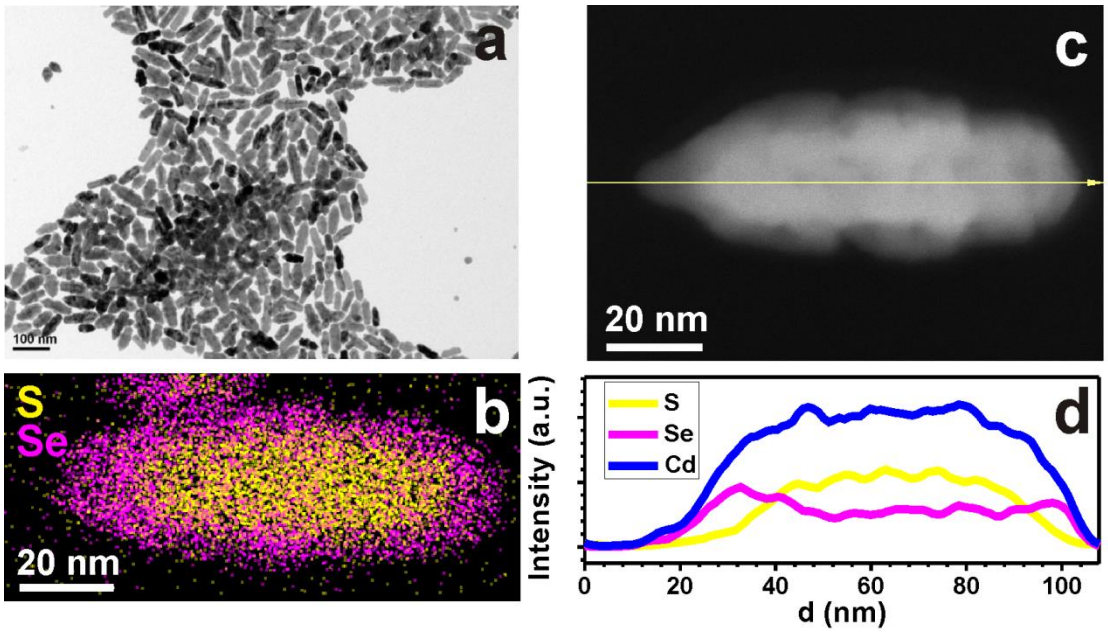

Figure S10. TEM analysis of the "reversed core-shell" rod-in-rod NCs, with $Cd_{1.6}S$(core)/$Cd_{0.97}S_{0.19}Se_{0.81}$(shell) composition according to EDS quantification. (a) Overview BF-TEM image of the NCs; (b) EDS map of Se (magenta) and S (yellow) for a single NC clearly demonstrating the reversed core-shell geometry; (c) HAADF-STEM image of one NC and (d) EDS line scan along the line drawn in (c) for Cd (blue), S (yellow) and Se (magenta) showing the enrichment of S at the core and Se at the periphery, with a homogeneous concentration of Cd along the NC.

Comparison of the valence bands for S and Se anion sublattices

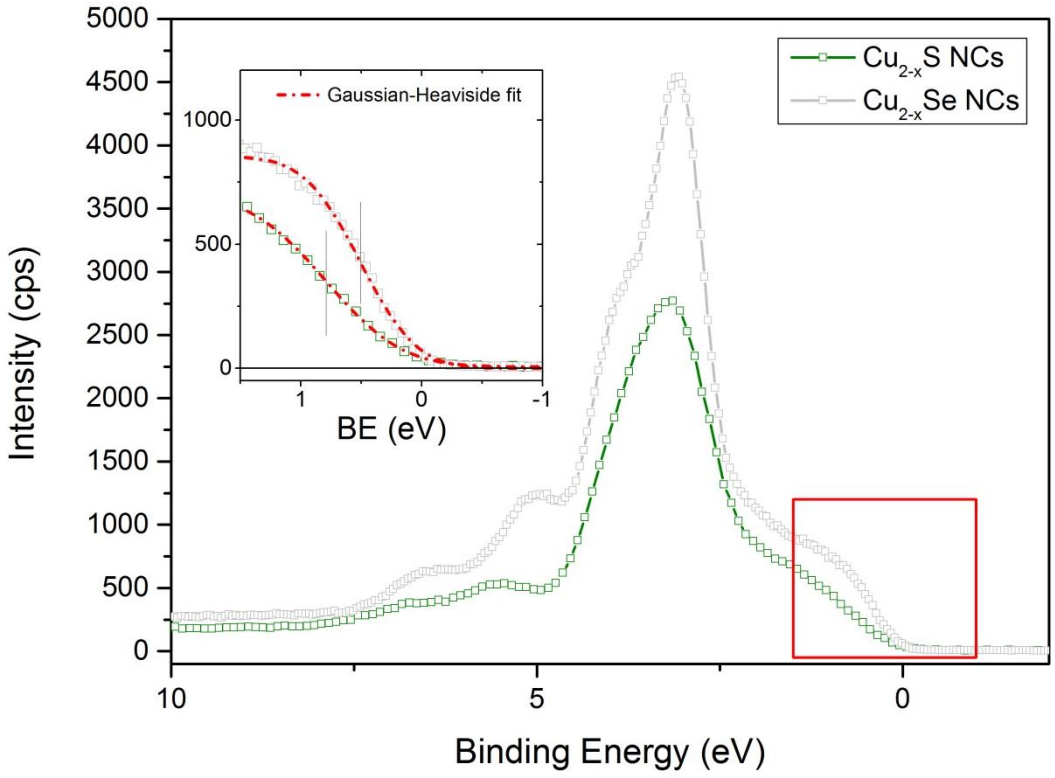

Figure S11: Valence band (VB) of $Cu_{2-x}S$ and $Cu_{2-x}Se$ NCs measured by XPS. The energy positions of the VB maxima are evaluated following the method reported in ref. [A. Santoni et al., J. Phys. D: Appl. Phys. 46 (2013) 175101], i.e. by modelling the VB onset with the convolution product of a Gaussian function and a Heaviside step function. This procedure was performed by using the built-in "Step down" background function in CasaXPS software [CasaXPS Manual – orange book - pg 292-295]; the obtained values are (0.8±0.1) eV and (0.5±0.1) eV, respectively for $Cu_{2-x}Se$ and $Cu_{2-x}S$ NCs, as indicated by the grey vertical bars in the inset.